Accepted Manuscript

Bio-inspired engineering of boron nitride with iron-derived nanocatalyst toward enhanced fire retardancy of epoxy resin

Zhi Li, Sara Isabel Montero Lira, Lu Zhang, Daniel Fernández Expósito, Vignesh Babu Heeralal, De-Yi Wang

PII: S0141-3910(18)30317-3

DOI: 10.1016/j.polymdegradstab.2018.10.005

Reference: PDST 8654

To appear in: *Polymer Degradation and Stability*

Received Date: 6 March 2018

Revised Date: 1 October 2018

Accepted Date: 7 October 2018

Please cite this article as: Li Z, Montero Lira SI, Zhang L, Expósito DanielFerná, Heeralal VB, Wang D-Y, Bio-inspired engineering of boron nitride with iron-derived nanocatalyst toward enhanced fire retardancy of epoxy resin, *Polymer Degradation and Stability* (2018), doi: https://doi.org/10.1016/j.polymdegradstab.2018.10.005.

Bio-inspired Engineering of Boron Nitride with Iron-derived Nanocatalyst toward Enhanced Fire retardancy of Epoxy Resin

Zhi Li [a,b], Sara Isabel Montero Lira [a,c], Lu Zhang [a,b], Daniel Fernández Expósito [a,d], Vignesh Babu Heeralal [a], De-Yi Wang [a*]

[a] *IMDEA Materials Insitute, C/Eric Kandel, 2, 28906 Getafe, Madrid, Spain*

[b] *Universidad Politécnica de Madrid, E.T.S. de Ingenieros de Caminos, 28040 Madrid, Spain*

[c] *Escuela Politécnica Superior (EPS), Universidad Carlos III de Madrid, Avda. de la Universidad, 30, 28911 Leganés, Madrid, Spain*

[d] *Escuela Superior de Ciencias Experimentales y Tecnología (ESCET),Universidad Rey Juan Carlos, C/Tulipán, s/n, 28933 Móstoles, Madrid, Spain*

[*]Corresponding author. Tel: +34 917871888

Email address: deyi.wang@imdea.org

Abstract

Aiming at improving fire retardancy of epoxy resin (EP), the thermal-exfoliated boron nitride nanosheets (BN) underwent the bio-inspired polydopamine (PDA) nano-coating and *in-situ* interfacial growth of iron-derived nanocatalyst (Fe) to prepare nanohybrid (BN@PDA@Fe). The design complied with principles: 1) PDA promoted the dispersion of BN in EP matrix and offered active sites for functionalization 2) bio-stabilized iron-derived nanoparticles catalyzed the polyaromatic reaction towards higher quality. Resultantly, 6wt% BN@PDA@Fe increased limiting oxygen index (LOI) of EP by 10.0% and suppressed fire spread in UL-94 test. The peak heat release rate (pHRR) was reduced by 38.9% with notably suppressed CO and smoke production. Ignition time, as a key aspect of fire safety, was effectively delayed due to enhanced thermal conductivity of BN-based EP nanocomposites. The optimization of char structure due to the interfacial charring accounted for the improved fire retardancy. In perspective, the bio-inspired engineering of BN offered a viable approach to improving fire safety of polymers.

Keywords: Boron nitride; Epoxy resin; Fire retardancy; Ignition; Interfacial charring

1. Introduction

Due to prominent thermal stability, mechanical property and superior flexibility in choosing monomers and curing agents, epoxy resin (EP) has aroused considerable focuses in the academic and industrial field. EP enjoys extensive applications in electric and electrical devices and laminates *etc*.[1]. However, the further utilization of EP is restricted especially in high-demanding circumstances due to its standard-below fire retardancy (ease of flammability) [2-5]. In order to address the issue, the prevailing nano-technique is capable to impart EP with satisfied fire retardancy and delayed ignition, accompanied by improved mechanical and thermal property [6, 7]. Recently, 0D nanoparticles (*e.g.*, silica [8]), 1D nanotubes (*e.g.*, carbon nanotubes [9, 10]) and 2D nanosheets (*e.g.*, layered double hydroxide [11] and graphene [12]) are evidenced as effective nanofillers to decrease fire hazard of polymers. Generally, 2D nanosheets exhibited a better fire retardancy compared with 0D and 1D nanofillers due to the formation of more protective carbonaceous layer [13].

Analogous to graphene nanoplatelets with carbon atom linked via sp^2, boron nitride nanosheets show lamellar structure with an equal quantity of boron and nitrogen atoms connected through sp^3 hybridization [14]. Resultantly, EP nanocomposite with boron nitride nanosheets was conferred with improved fire safety in terms of delayed ignition time (TTI), reduced heat release and smoke production [15-17]. Compared with other nanofillers [18-20], boron nitride nanosheets presented the superiority in simultaneously delaying ignition and reducing heat release of polymers [14, 21]. However, in order to promote fire-retardant efficiency, the organic functionalization with cyclotriphosphazene on boron nitride surface was performed [21]. In comparison, the rarely reported inorganic modification on the surface of boron nitride nanosheets (surface modification) enabled to offer an alternative to ameliorate fire hazard of EP matrix. It was expected that the interfacial (or surface) location of nanocatalyst between EP matrix and BN nanosheets contributed to the catalytic charring of EP matrix, which resulted in the optimized char structure [22]. However, the direct

growth of inorganic nanoparticles on boron nitride nanosheets encountered difficulty owing to the lacking of essential active sites. Fortunately, the dopamine chemistry presented the strong bio-adhesion toward inert surface with polydopamine (PDA) as the bridging nano-layer. The result was the inhibition of aggregation of boron nitride nanosheets in polymer matrix, favoring the thermal stability and conductivity [23]. In parallel, the presence of PDA on BN nanosheets facilitated the interfacial growth of inorganic nanomaterials due to the intensive coordination interaction. Iron-derived nanoparticles (Fe) were regarded as excellent charring catalyst toward polyaromatic reaction of pyrolyzed products of EP in consideration of the intensive Lewis acidic sites [22]. The fire retardancy was profited after the incorporation of Fe on boron nitride surface, which combined the prominent barrier effect of boron nitride against external heat and the catalytic charring capacity of Fe nanocatalyst. Meanwhile, the thermal exfoliation of boron nitride nanosheets was evidenced to possess more active sites and favor the dispersion in EP matrix [14]. Herein, the thermally exfoliated boron nitride will perform as the substrate for sequential functionalization rather than pristine boron nitride.

Aiming to impart EP matrix with enhanced fire retardancy, the bio-inspired sequential engineering of thermally exfoliated boron nitride nanosheets (BN) with PDA and iron-derived nanocatalyst were executed and verified successfully. The dispersion of nanofillers in EP matrix was investigated via X-ray diffraction (XRD) and scanning electron microscopy (SEM). The fire retardancy was investigated by limiting oxygen index (LOI), UL-94 horizontal burning test and cone calorimeter test (CCT). The condensed-phase mechanism was analyzed via digital image, SEM and XRD. The thermal degradation was probed by thermogravimetric analyzer (TG) and thermogravimetric analyzer coupled with Fourier transform infrared spectra (TG-FTIR). The thermal conductivity was analyzed to account for the ignition behavior.

2. Experimental

2.1 Chemicals

Hexagonal boron nitride powder (h-BN), condensed hydrochloric acid (HCl, 37wt%), dopamine hydrochloride (DA·HCl), tris(hydroxymethyl)aminomethane (tris), iron (Ⅲ) chloride ($FeCl_3$), sodium borohydride ($NaBH_4$) and diethylenetriamine (DETA) were bought from Sigma-Aldrich. Epoxydharz C was purchased from Faserverbundwerkstoffe Composite Technology Company as epoxy resin monomer. Tris(hydroxymethyl)aminomethane buffer solution with pH value of 8.5 and concentration of 0.05mol/L was prepared in our lab. Deionized water was prepared in our institute.

2.2 Thermal exfoliation of h-BN and its PDA functionalization

In the typical procedure, the exfoliated BN nanosheets (BN) were obtained after thermal-oxidation exfoliation with treatment of h-BN powder at 1000^{o}C in tubular furnace under air atmosphere [24]. Subsequently, 10g exfoliated BN nanosheets were charged into 1L three-neck flask with 800mL buffer solution. The ultrasonication treatment was applied for 30min prior to addition of 2g DA·HCl with vigorous stirring. The encapsulation and polymerization process occurred with colour turning black (**Scheme 1**). After the reaction for 24h, the products (BN@PDA) were collected after vacuum filtration, washing with deionized water and drying overnight. The weight percentage of PDA in BN@PDA was measured as 11.2wt%.

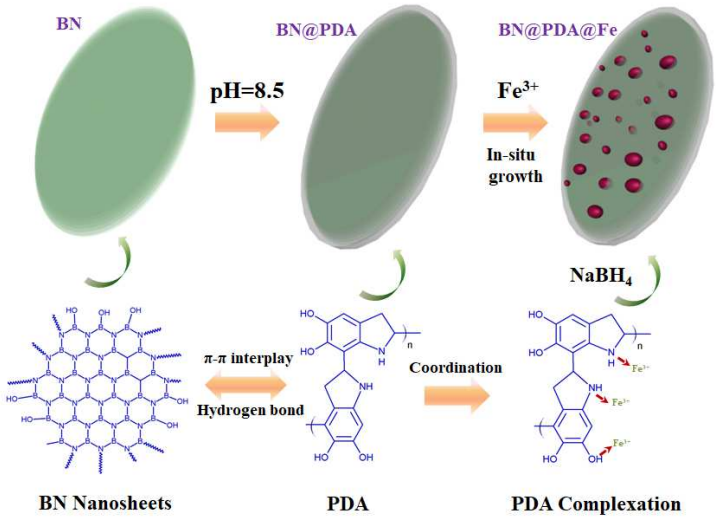

Scheme 1 Preparation route of BN@PDA and BN@PDA@Fe

2.3 *In-situ* growth of iron-derived nanoparticles on BN@PDA (BN@PDA@Fe)

10g BN@PDA was dispersed into 350mL deionized water prior to the ultrasonication for 30min. Subsequently, the addition of 2g $FeCl_3$ was carried out with vigorous stirring. In order to guarantee the coordination of Fe^{3+} and PDA molecules, the reaction persisted for 3h, followed by the drop-wise addition of $NaBH_4$ solution (1g $NaBH_4$ and 50mL water). During the slow dripping, the bubbles were generated, which inferred the reduction of Fe^{3+}. After additional 30min reaction, the materials were filtrated and washed with deionized water for several times. Finally, the product was obtained after vacuum drying overnight and labelled as BN@PDA@Fe. The procedure was illustrated in **Scheme 1**. The percentage of iron derivatives was measured as 5.7wt% in BN@PDA@Fe.

2.4 Preparation of EP nanocomposites

EP nanocomposites with the fraction of 6wt% BN, BN@PDA and BN@PDA@Fe were respectively prepared. In the typical procedure, EP monomer was mixed with nanofillers at 60^{o}C to acquire the preliminary dispersion. Subsequently, the triple-milling treatment was applied to generate the better nano-dispersion under the strong shear. With vigorous stirring, the curing agent DETA with stoichiometric amount was added to mixture, after which the degas treatment was executed using the ultrasonication for 5min. The degassed mixture was then casted into the silicon mold prior to the static curing process for 24h at ambient temperature. After the ambient curing, the resultant samples were transferred for heated curing at 120^{o}C for additional 2h. In parallel, the neat EP was fabricated via the identical steps.

2.5 Instrumental

Raman spectra were recorded in Raman spectroscopy (Renishaw PLC) with a 532nm Nd:YAG laser (50mW at 532 nm). X-ray diffraction (XRD) was conducted in diffractometer (Empyrean, PANalytical) with Cu Kα X-ray source and Ni filter. X-ray photoelectron spectroscopy (XPS) was conducted on VG ESCALAB MK II spectrometer with Al Kα radiation. Scanning electron microscopy (SEM) was performed on EVO MA15, Zeiss with EDS (Oxford INCA 350). Transmission

electron microscopy (TEM) was carried out on FEG S/TEM microscopy (Talos F200X, FEI) under the accelerating voltage of 200kV. STEM mode was employed to analyze element and element distribution. Thermogravimetric analysis (TG) was recorded on equipment (Q50, TA Instruments) at 10^{o}C/min from ambient temperature to 800^{o}C. Thermogravimetric analyzer coupled with Fourier transform infrared spectra (TG-FTIR) were conducted on FTIR spectrometer (Nicolet iS50) connected with TG analyzer (Q50, TA Instruments) through a heated pipe. The constant weight (15±0.2mg) sample underwent the heating from ambient temperature to 800^{o}C at 10^{o}C/min. The evolved volatiles were directed to gas chamber for FTIR measurement. Limiting oxygen index (LOI, FTT) was carried out according to D2863-2013 on samples with 12.7mm×6.5mm×3.0 mm. UL-94 horizontal burning test (FTT) was performed on samples with 127.0mm×12.7 mm×3.0mm. The horizontal samples were flamed 25s prior to analysis by spread rate. Cone colorimeter test (CCT, FTT) was used to characterize the combustion behavior on samples with 100.0mm×100.0mm×4.0mm under 35kW/m^2 according to ISO 5660-1. The ignition behavior (time to ignition, TTI) was analyzed in CCT. At least 2 specimens were tested for average values. Thermal conductivity was conducted in Hot Disk Thermal Constants Analyzer (Switzerland).

3. Result and discussion

3.1 Characterization of targeted BN@PDA@Fe

Raman and XRD spectra

Raman and XRD spectra were illustrated in **Fig.1**. In terms of BN in **Fig.1** (a), the peak at 1366 cm^{-1} was attributed to E_{2g} tangential mode. The PDA modification on BN surfaces generated an additional peak at 1606cm^{-1}, which was originated from the catechol structure of PDA macromolecules [25]. Moreover, the fitting of the new peak gave rise to two different peaks at 1570 cm^{-1} and 1618 cm^{-1} with assignments to the deformation and stretching vibration of the catechol structure respectively [26]. Actually, the catechol structure was apt to form the π-π interaction with six-member ring structure of BN, which favoured the bio-adhesion and encapsulation. The polar

and hydrophilic groups (-OH) in activated BN also facilitated the adhesion via hydrogen-bond. However, the invariable location of E_{2g} tangential mode with PDA functionalization showed that the π-π interaction was relatively weak. Furthermore, the incorporation of Fe component shifted the peaks at 1570 cm^{-1} and 1618 cm^{-1} toward the lower locations of 1555 cm^{-1} and 1606 cm^{-1} separately. The red shift of the deformation and stretching vibration was due to the coordination effect between Fe and PDA [26]. The coordination effect facilitated the vibration shift toward low-energy state for the structural stabilization [22].

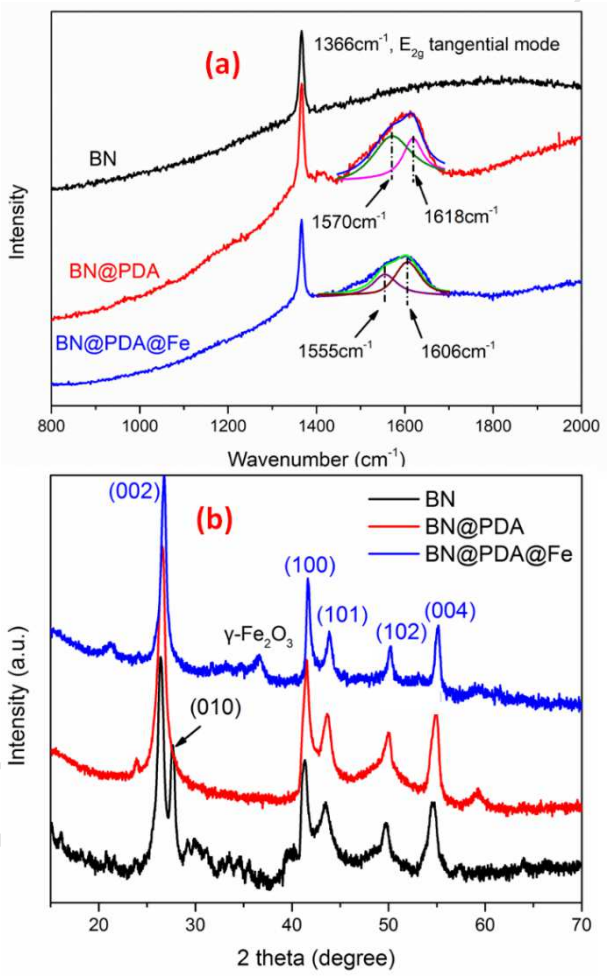

Fig.1 (a) Raman Spectra and (b) XRD spectra of BN, BN@PDA and BN@PDA@Fe

XRD pattern (**Fig.1** (b)) of thermally exfoliated boron nitride nanosheets (BN) exhibited the peaks at 26.4°, 27.2°, 41.2°, 43.5°, 49.6° and 54.6°, which were assigned to the crystal faces of (002), (010), (100), (101), (102) and (004) respectively. Additionally, compared with the pristine BN, the new peak at 27.2° from (010)

reflection of $B(OH)_3$ was due to the high-temperature thermal exfoliation [14, 24]. After the PDA encapsulation, all the peaks of BN persisted with the exception of $B(OH)_3$ reflection. The possible cause for the disappearance of $B(OH)_3$ reflection was due to the compression-derived shrinkage from encapsulation. In parallel, the Fe nanocatalyst on BN@PDA gave rise to additional peaks at 36.5^o, which was corresponded to γ-Fe_2O_3 [27]. According to the preparation of BN@PDA@Fe, the reduction of Fe^{3+} instantly generated zero-valent iron (Fe^0), followed by the oxidation to γ-FeOOH and subsequent dehydration to γ-Fe_2O_3. The relatively large peak size at 36.5^o illustrated that γ-Fe_2O_3 constituted the major part of the nanocrystal.

XPS spectra

Aiming to further confirm the composition of BN@PDA@Fe, XPS measurement was performed and showed in **Fig.2**. In **Fig.2** (a), the full XPS spectra illustrated the inclusion of B, N, C, Fe and O in BN@PDA@Fe. O1s peak fitting in **Fig.2** (b) displayed the C=O and C-O bands at 331.5eV and 332.5eV, which were attributed to catechol structure. N1s fitting results in **Fig.2** (c) manifested the presence of different N sources of BN and PDA. Fe 2p spectra certified the presence of a trace of zero-valent iron (706.5eV) and γ-Fe_2O_3 (Fe2p3/2 at 712.2eV and Fe2p1/2 at 725.8eV) [28].

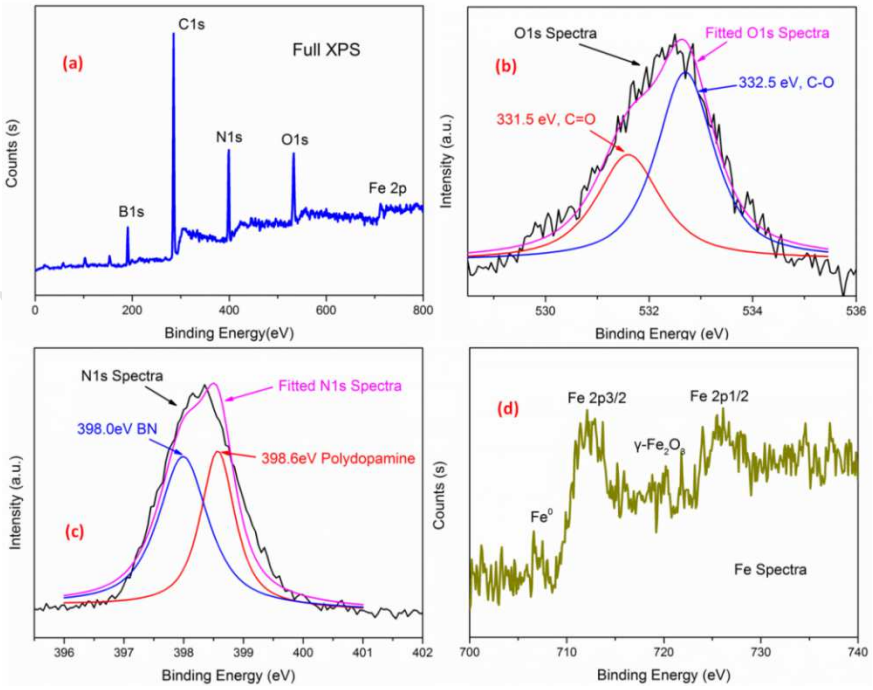

Fig.2 (a) Full XPS spectra; (b) O1s spectra; (c) N1s spectra and (d) Fe2p spectra of BN@PDA@Fe

TEM and EDS analysis

In SEM images (**Fig S1** (a) and (b)), the bio-inspired engineering of PDA on thermally exfoliated boron nitride nanosheets (BN) did not influence the morphology. In contrast, the incorporation of Fe nanocatalyst on the surface of BN@PDA generated slight alteration with stretched nanosheet (red circles in **Fig S1** (c)).

In TEM images (**Fig.3** (a)), BN possessed lamellar structure with lateral size in micron-scale and thickness in nano-scale. The analysis of BN edge in **Fig.3** (a) and the inset selected area electron diffraction (SAED) revealed the ordered stacked structure. The combination of the ordered structure and the single-sheet BN in **Fig.3** (d) reflected the limited thermal exfoliation. Meanwhile, the high angle annular dark field (HAADF) image with B and N mapping (**Fig.3** (e)) and O mapping (**Fig.3** (f)) presented the consistent results with XPS results, which evidenced the successful thermal-oxidation exfoliation of BN. In parallel, the PDA encapsulation of BN generated obscure edge (**Fig.3** (b) and (g)) without notable change in SEAD patterns (inset in **Fig.3** (b)). The formation of obscure edge revealed the encapsulation of BN surface by PDA nano-coating. Also, the retained SEAD patterns demonstrated the absence of the exfoliation of lamellar structure of BN. In parallel, in **Fig.3** (c) and (h), Fe nanocatalyst was successfully dispersed on BN@PDA in the strip shape, which indicated that the Fe nanocrystal grown along the specific direction. In **Fig.3** (i) with higher magnification, some irregular Fe nanocatalysts were surrounding the nano-strips, which revealed the disordered dispersion of Fe nanocatalyst. Moreover, the exploration of **Fig.3** (i) verified the main component of γ-Fe_2O_3 in the Fe nanocatalyst, which was in a good agreement with the XRD result.

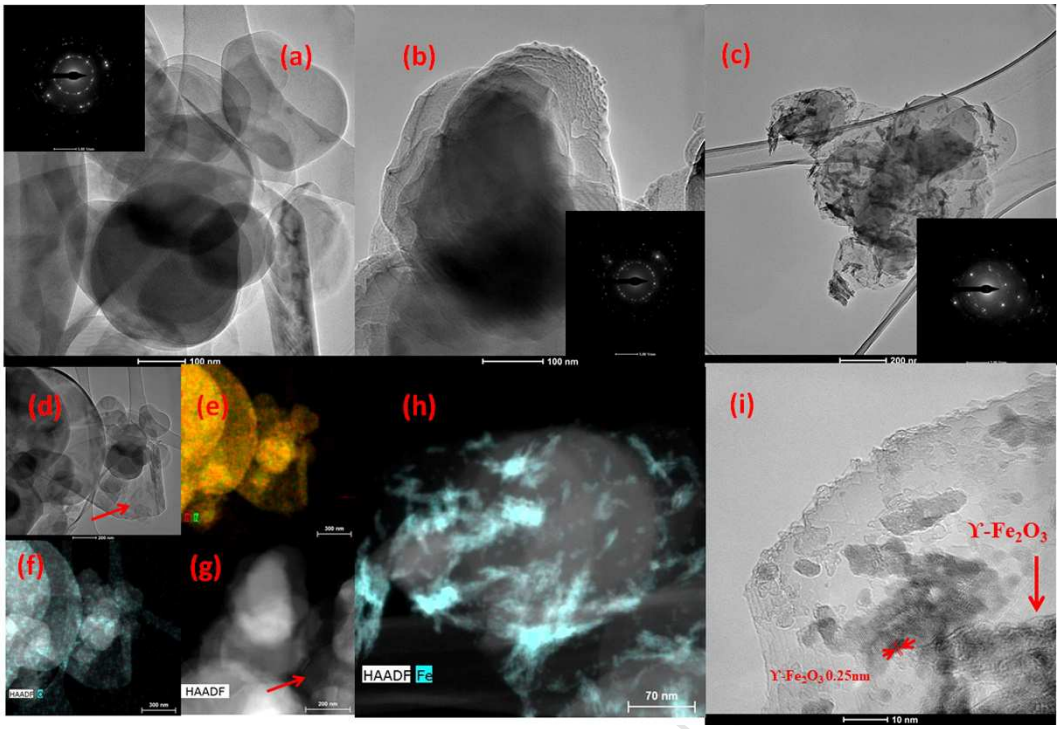

Fig.3. TEM images with of (a) and (d) BN, (b) BN@PDA and (c, i) BN@PDA@Fe with the inset SAED; (d) High angle annular dark field (HAADF), (e) B and N mapping and (f) O mapping of thermally exfoliated BN; (g) HAADF mapping of BN@PDA, (h) Fe mapping of BN@PDA@Fe

3.2 Dispersion state of EP nanocomposites

XRD pattern

EP, EP/6BN and EP/6BN@PDA@Fe were selected for bulk XRD test (**Fig.4**) in consideration of the similar blending property of BN@PDA and BN@PDA@Fe. The peaks emerged at around 18.5^{o} and 41.2^{o}, which were characteristic of EP matrix. After the addition of BN and BN@PDA@Fe, the peaks of EP matrix retained. Additionally, BN and BN@PDA@Fe brought extra peaks located at 26.4^{o}, which was assigned to (002) crystal face of BN. The invariable location of (002) reflection demonstrated that the lamellar BN nanosheets were not intercalated or completely exfoliated during processing and curing process, which was consistent with limited thermal exfoliation in XRD (**Fig.1**) and TEM image (inset in **Fig.3** (c)).

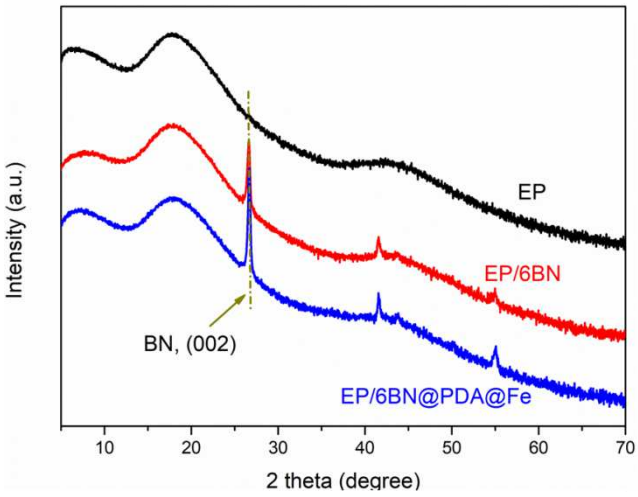

Fig.4. XRD patterns of EP, EP/6BN and EP/6BN@PDA@Fe

SEM observation

The dispersion state of nanofillers in EP matrix was further investigated by SEM (**Fig.5**). EP matrix possessed relatively smooth cryo-fractured surface (**Fig.5** (a)). The addition of BN generated notable wrinkled surface with the aggregates of BN, which were confirmed by EDS spectra (**Fig S2**) and B mapping (inset in **Fig.5** (b)). The EDS spectra presented the asymmetric shape with the preferential B peak in the left side. In parallel, the PDA modification of BN generated slightly more wrinkled surface with better BN nano-dispersion (marked with arrows) (**Fig.5** (c)). EP/6BN@PDA@Fe illustrated more wrinkled surface than that of EP/6BN@PDA with more uniform nano-dispersion in EP matrix (marked with arrays). Hence, BN, BN@PDA and BN@PDA@Fe demonstrated increasingly better nano-dispersion state in EP matrix. In combination of XRD results, BN@PDA@Fe revealed more uniform dispersion in EP matrix (**Fig.5** (e) and (f)) but not more exfoliation relative to BN and BN@PDA.

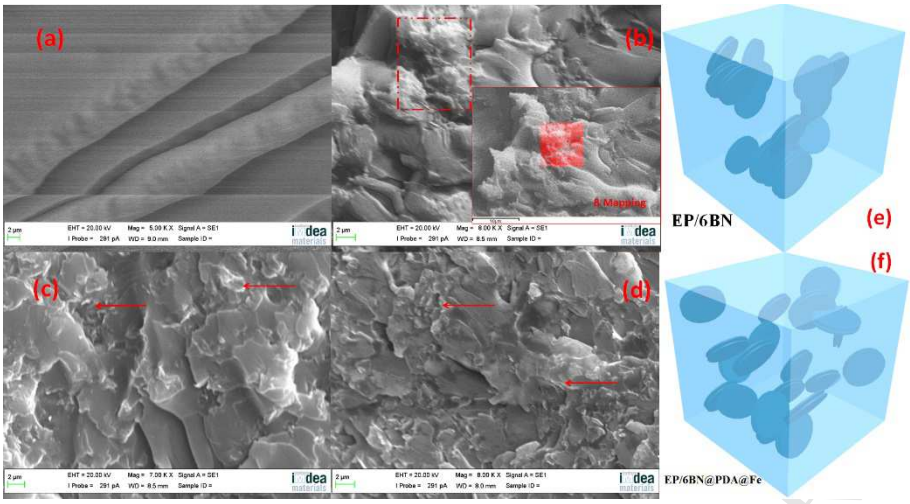

Fig.5. Cryo-fractured surface of (a) EP, (b) EP/6BN with inset EDS spectra and B mapping of selected area, (c) EP/6BN@PDA with inset B mapping of selected area and (d) EP/6BN@PDA@Fe; schematic illustration of (e) EP/6BN and (f) EP/6BN@PDA@Fe

3.3 Thermal stability

The thermal stability was exhibited in **Table 1** and **Fig.6** at N_2 atmosphere. The addition of BN and BN@PDA did not change the $T_{5wt\%}$ and $T_{50wt\%}$ notably, which indicated that the initial thermal stability of EP matrix was maintained [29]. Meanwhile, the calculation was carried out through the simple numerical combination of EP matrix and nanofillers (BN and BN@PDA) (**Fig S3** (a) and (b)). The calculated char yield at 650^{o}C of EP/6BN reached 16.1wt%, which was notably lower than experimental values (18.3wt%). Reasonably, the increase of experimental char yield relative to the calculated value was attributed to the barrier effect of lamellar BN toward heat and volatiles. In terms of EP/6BN@PDA, the calculated char yield of 15.9wt% was close to the experimental value of 16.7wt%. In the experimental TG curves (**Fig.6** (a)), the PDA modification slightly decreased char yield at 650^{o}C compared with EP/6BN even though the better nano-dispersion of BN@PDA (**Fig.5** (c)) was formed. In order to clarify the underlying reason why the PDA encapsulation exerted the notable effect on the thermal degradation of EP/6BN, PDA microspheres were prepared via the modified oxidation polymerization [30]. The investigation of TG curve of PDA and the calculated TG curve of EP/6BN@PDA (**Fig.6** (b)) (from the

numerical combination of EP/6BN and PDA) illustrated that the PDA component was able to degrade over the test temperature and probably deteriorate the char structure and barrier effect of EP/6BN [31]. Meanwhile, the relatively high percentage of PDA in BN@PDA also played a critical role in promoting the damage.

The growth of Fe on BN@PDA slightly decreased the initial thermal stability ($T_{5wt\%}$, 328^{o}C) and $T_{50wt\%}$, which manifested that Fe nanocatalyst promoted the thermal degradation of EP matrix at the initial and medium stage [22]. In a general sense, the earlier thermal degradation facilitated the charring effect, which was beneficial to fire retardancy [32]. The comparison of experimental and calculated char yield of EP/6BN@PDA@Fe in **Table 1** illustrated the barrier effect of BN@PDA@Fe in EP matrix. Compared with that of EP/6BN@PDA, the char yield of EP/6BN@PDA@Fe at 650^{o}C was 19.8wt%, which displayed a 3.1wt% increment. The incorporation of Fe promoted the catalytic charring behavior of EP/6BN@PDA via overcoming the high-temperature instability of PDA. The increased char yield played an important role in fire retardancy based on the formation of more robust carbonaceous layer [33-35].

Table 1 TG result of EP, EP/6BN, EP/6BN@PDA and EP/6BN@PDA@Fe

	$T_{5wt\%}$ (^{o}C)	$T_{50wt\%}$ (^{o}C)	CY (%) at 650^{o}C	Calculated CY (%) at 650^{o}C
EP	336	373	10.7	10.7
EP/6BN	336	375	18.3	16.1
EP/6BN@PDA	335	377	16.7	15.9
EP/6BN@PDA@Fe	328	363	19.8	15.8

$T_{5wt\%}$: Temperature at 5% mass loss $T_{50wt\%}$: Temperature at 50% mass loss CY: char yield

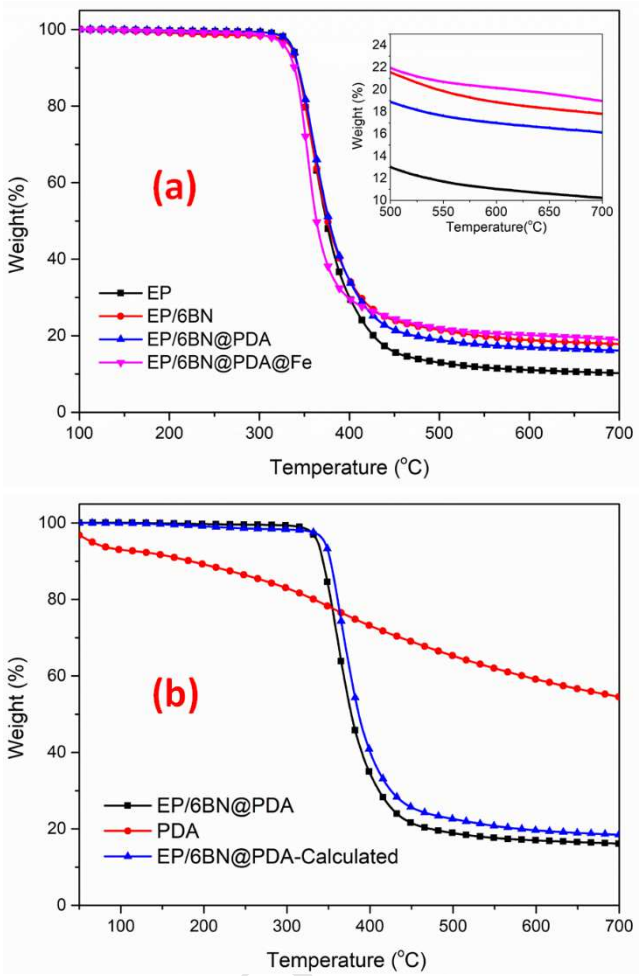

Fig.6 (a) TG curves of EP and EP nanocomposites at N_2 atmosphere; (b) TG curve of PDA and calculated TG curve of EP/6BN@PDA

3.4 Combustion behavior

LOI investigation

The LOI result was showed in **Fig.7** (a). Compared with neat EP (24.2%), EP/6BN, EP/6BN@PDA and EP/6BN@PDA@Fe possessed the increased LOI value to 31.2%, 28.5% and 34.2% respectively. The addition of BN into EP matrix increased LOI value, which was attributed to the dominant barrier effect against heat and volatiles as well as the increased thermal conductivity (**Fig.7** (b)). The char of EP/6BN shielded the heat and flammable gases, interrupting the combustion. From another aspect, the increased thermal conductivity possibly had a stronger effect than the increased flammable gases from the thermal degradation of underlying EP matrix, which

resulted in the stronger heat dissipation and extinguished the fire. In contrast, the PDA functionalization unexpectedly decreased the LOI value of EP/6BN despite thermal conductivity was increased. The probable reason was originated from the worse char quality, incited by high-temperature instability of EP/6BN@PDA (**Fig.6** (a)). The continuous thermal degradation of PDA (at the interface between EP and BN) damaged the char structure and barrier effect of EP/6BN with more transportation of heat and flammable gases (**Fig.6** (b)).

In contrast, the incorporation of Fe nanocatalyst increased LOI value by 5.7% relative to that of EP/6BN@PDA. The thermal conductivity of EP/6BN@PDA and EP/6BN@PDA@Fe remained almost equal. In the sense, the improved char quality with higher char yield (**Fig.6** (a)) probably accounted for enhanced LOI value of EP/6BN@PDA@Fe relative to that of EP/6BN@PDA. The comprehensive investigation of relationship between LOI value and the char at 650^{o}C of EP, EP/6BN, EP/6BN@PDA and EP/6BN@PDA@Fe implied that the char yield and barrier effect played a more important role during combustion. Apart from it, the addition of 6wt% BN@PDA@Fe increased the thermal conductivity by 29.9% to 0.339 W m^{-1} K^{-1} compared with EP, which offered alternative routes to manage the heat behavior [23].

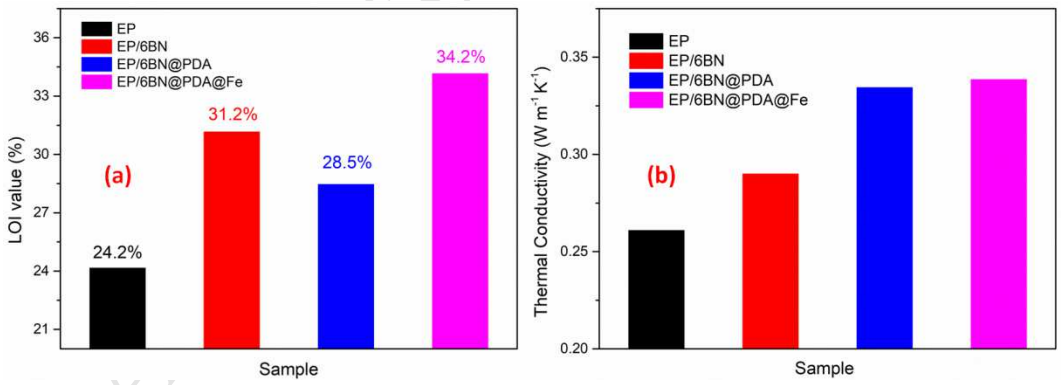

Fig.7 (a) LOI values and (b) thermal conductivity of EP and EP nanocomposites

UL-94 horizontal burning test

In UL-94 horizontal burning test (**Fig S4**), EP and EP nanocomposites possessed the self-extinguishing feature with the difference in burning length and time. At 44s, EP/6BN and EP/6BN@PDA@Fe generated slightly weaker fire than EP and

EP/6BN@PDA, which was in good consistency with LOI result. As the flame was in the critical point of self-extinguishment, EP, EP/6BN, EP/6BN@PDA and EP/6BN@PDA@Fe took the burning time of 3min 55s, 1min 30s, 1min 56s and 1min 16s, correspondingly. In parallel, the burning length (marked in red dot-line rectangle) revealed the burning sequence of EP>EP/6BN@PDA>EP/6BN>EP/6BN@PDA@Fe. The burning time and length demonstrated that BN improved fire retardancy of EP but PDA modification deteriorated fire retardancy. The growth of Fe nanocatalyst enhanced fire retardancy with stronger self-extinguishment.

Cone calorimeter test

Cone calorimeter test (CCT) is considered as the closest forced flame test to realistic fire scenario [29, 36]. Herein, the CCT result was presented in **Fig.8** and **Table 2**. In HRR curves (**Fig .8** (a)), two peaks inviably emerged in terms of the four samples, which indicated the generation, damage and reconstruction of carbonaceous layer. The addition of 6wt% BN, BN@PDA and BN@PDA@Fe changed the pHRR value of EP (1208±45 kW/m^2) to 907±32 kW/m^2, 1158±39 kW/m^2 and 738±27 kW/m^2 respectively. Amongst them, BN@PDA@Fe after the sequential functionalization of PDA and Fe nanocatalyst imparted EP matrix with the most significantly reduced pHRR by 38.9%. However, the single-step PDA modification unexpectedly increased pHRR value relative to EP/6BN which was in agreement with LOI and TG results.

In parallel, the fire growth index (FIGRA), which was defined as the pHRR divided by time to pHRR, illustrated the fire-growth behavior of polymers. EP/6BN@PDA@Fe possessed FIGRA of 4.59 kW/(m^2·s), which was notably reduced compared to EP (6.75 kW/(m^2·s)), EP/6BN (4.72 kW/(m^2·s)) and EP/6BN@PDA (7.65 kW/(m^2·s)). Reasonably, the remarkable reduction of FIGRA implied the suppression effect of fire growth of EP via the sequential modification of BN. Moreover, the study of THR at 350s (**Fig.8** (b)) disclosed that EP/6BN@PDA@Fe possessed lower value of 83.2±2.5 MJ/m^2 than EP (14.6% reduction), EP/6BN (5.8% reduction) and EP/6BN@DPA (22.0% reduction). The average mass loss rate (AMLR) was employed to assess the fire behavior. In **Fig. 8** (c), EP/6BN@PDA@Fe had

AMLR value of 0.085 g/s, which was reduced by 34.6%, 9.6% and 34.7% respectively compared with EP, EP/6BN and EP/6BN@PDA. The lower AMLR value illuminated the lower fire intensity. In parallel, the char yield at flameout of EP/6BN@PDA@Fe was 29.0%, 11.3% and 21.2% higher than EP, EP/6BN and EP/6BN@PDA4 separately, which was in consistency with the char yield in TG (**Fig.6** and **Table 1**). The lower char yield after PDA modification relative to EP/6BN was due to the triggering effect of PDA located at the interface of BN and EP towards worse char-stability. In contrast, the incorporation of Fe improved charring capacity of EP/6BN@PDA via catalytic process.

Time to ignition (TTI) was an important indicator that reflected fire hazard according to the standard ISO/IEC 13943. Compared with neat EP (80±3 s), the addition of BN notably increased TTI to 102±3 s (27.5%), which was strongly related to the enhanced thermal conductivity. Reasonably, the heat imposed on the surface was conducted to underlying layers more swiftly prior to ignition in terms of EP/6BN, thus resulting in less temperature on the surface. The PDA modification on BN did not change TTI noticeably even through the thermal conductivity was increased. The reason was possibly due to the decreased specific heat of capacity, which compensated the impact of thermal conductivity. The incorporation of Fe nanocatalyst slightly reduced TTI value to 89±1 s compared with 98±3 s of EP/6BN@PDA, which disclosed the critical influence of thermal degradation on TTI based on the almost identical thermal conductivity. However, compared with neat EP, EP/6BN@PDA@Fe possessed the delayed TTI by 9s, which revealed that the ignitability turned more difficult with lower fire hazard.

Table 2 CCT data of EP and EP composites (35kW/m^2)

Sample	TTI(s)	pHRR (kW/m^2)	THR (MJ/m^2) at 350s	TSP(m^2) at 350s	AMLR (g/s)	FIGRA (kW/(m^2 • s))
EP	80±3	1208±45	97.4±3.7	21.5±0.9	0.130±0.007	6.75
EP/6BN	102±3	907±32	88.3±3.1	18.2±1.3	0.094±0.006	4.72
EP/6BN@PDA	98±3	1158±39	106.7±4.2	22.4±1.4	0.131±0.006	7.65
EP/6BN@PDA@Fe	89±1	738±27	83.2±2.5	14.5±0.5	0.085±0.003	4.59

TTI: Time to ignition pHRR: Peak heat release rate THR at 350s: Total heat release at 350s

TSP at 350s: Total smoke production at 350s AMLR: Average mass loss rate FIRGA: Fire growth index

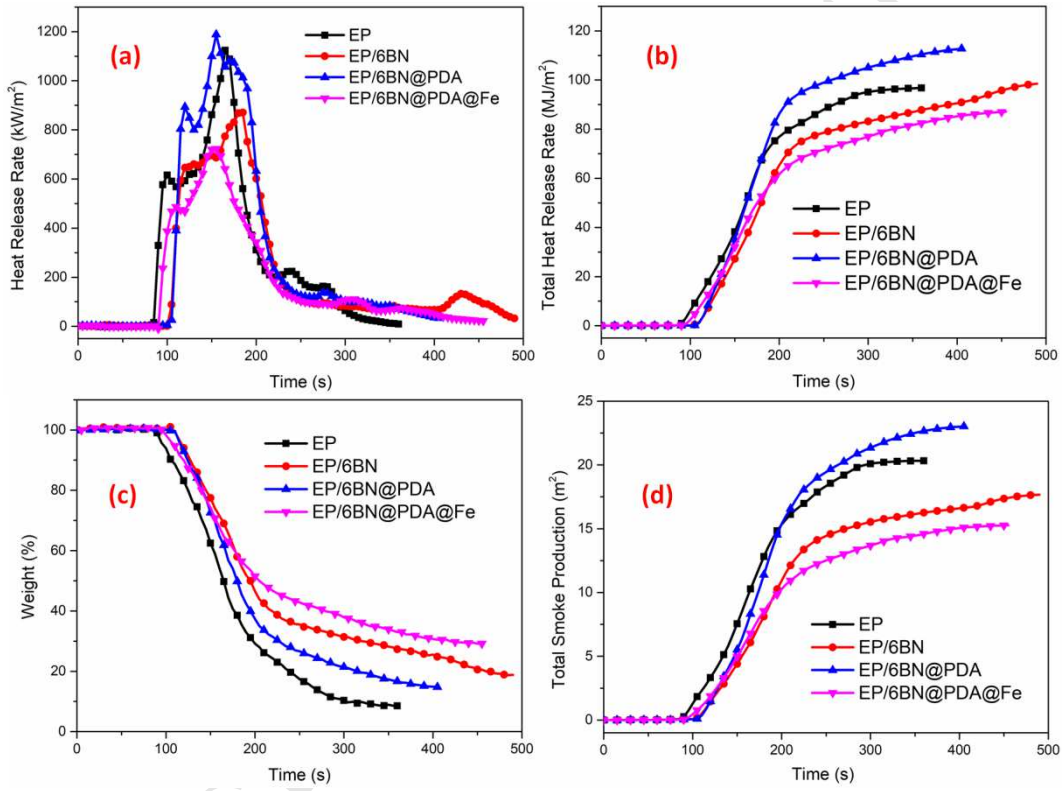

Fig.8 (a) HRR, (b) THR, (c) weight profile and (d) TSP of EP and EP nanocomposites

As another component of fire safety, the smoke profile was investigated in **Fig. 8** (d) and **Fig S5**. The smoke production rate (SPR in **Fig S5**) exhibited the similar trend as HRR, which demonstrated the typical condensed-phase smoke-suppression behavior. Total smoke production (TSP) value in **Fig.8** (d) at 350s of EP/6BN@PDA@Fe was 14.5±0.5 m^2, which was reduced by 32.6% compared to neat EP. Additionally, carbon monoxide (CO) production was the important constituent in fire safety. In **Fig.9** (a), EP/6BN@DPA@Fe possessed the peak CO production rate of 0.025±

0.001g/s, which was 40.1%, 16.7% and 39.0% lower than those of EP (0.042± 0.002g/s), EP/6BN (0.030 ± 0.001g/s) and EP/6BN/PDA (0.041 ± 0.002g/s) respectively. Similarly, the PDA modification deteriorated CO profile with higher peak CO production rate relative to EP/6BN. In parallel, the released amount of CO (**Fig.9** (b)) illustrated the similar trend to peak CO production with the CO weight at 350s of EP/6BN@PDA@Fe 2.2±0.1g compared to 3.1±0.1g of neat EP. **Fig.9** (c) demonstrated the delayed and reduced ratio of COP and CO_2P of EP/6BN@PDA@Fe compared to neat EP at the after-flame stage. The delayed and reduced ratio of COP and CO_2P revealed the suppressed CO production relative to CO_2 production at the after-flame stage. In particular, the incorporation of iron nanocatalyst into EP/6BN@PDA suppressed the CO production relative to CO_2 production due to the catalysis of iron, which was in agreement with the previous report probably [37]. Conclusively, the sequential functionalization of BN by PDA and Fe reduced the fire hazard of EP.

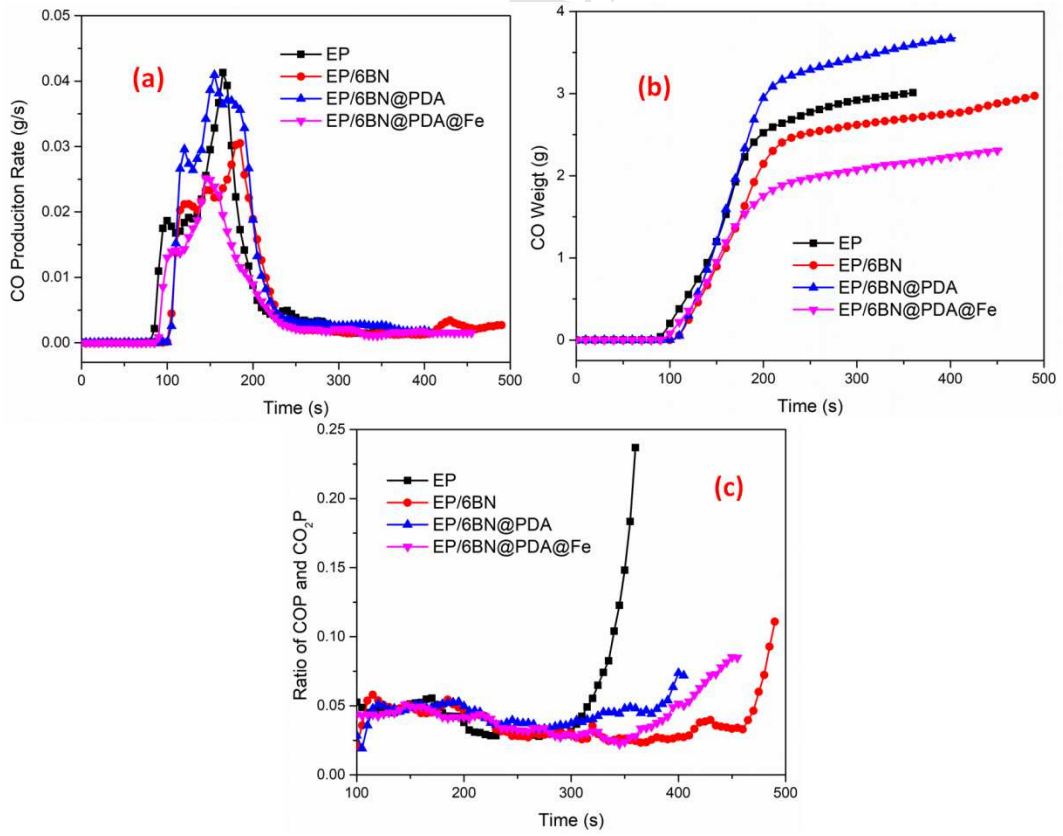

Fig.9 (a) CO production rate, (b) weight of CO production and (c) ratio of COP and

CO_2P of EP, EP/6BN, EP/6BN@PDA and EP/6BN@PDA@Fe

In order to study the cause to better fire safety with BN@PDA@Fe, the char after CCT was visually analyzed in **Fig .10** and **Fig S6**. EP generated a small amount of char with isolated and loose structure (**Fig.10** (a1) and (a2)). The incorporation of BN resulted in a larger amount of char with closer stacking and more compact structure (**Fig.10** (b1) and (b2)). SEM image showed fluffy surface that contained the naked particles and macroscopic pores (**Fig S6** (b)). After the PDA modification, the char possessed the hollows in the center with loosely stacked char pieces (**Fig.10** (c1) and (c2)). SEM observation of the interior surface illustrated that naked BN particles partially merged into surface with unexpected generation of more holes relative to EP and EP/6BN (**Fig S6** (c)). The probable cause was closely correlated to the continuous thermal degradation of PDA component. It was reasonable that compared to EP/6BN, the char from EP/6BN@PDA generated less protection towards the underlying undecomposed EP matrix. The incorporation of Fe nanocatalyst on BN@PDA gave rise to continuous and compact char structure with less fracture, which was regarded as the excellent carbonaceous layer structure (**Fig.10** (d1) and (d2)). SEM analysis (**Fig S6** (d)) revealed that even though the holes were maintained, the naked and undamaged BN nanosheets (evidenced by XRD in **Fig S7**) were almost embedded into char. Even though the detected fluffy char structure was present, the more continuous and compact char structure possessed the better performance in resisting the penetration of external heat and volatiles. At the microscale, the newly-formed char due to the possible interfacial catalysis covered on BN surface, which promoted the reinforcement effect of BN nanosheets. Imaginarily, the improved solid char structure compensated the impact of the holes.

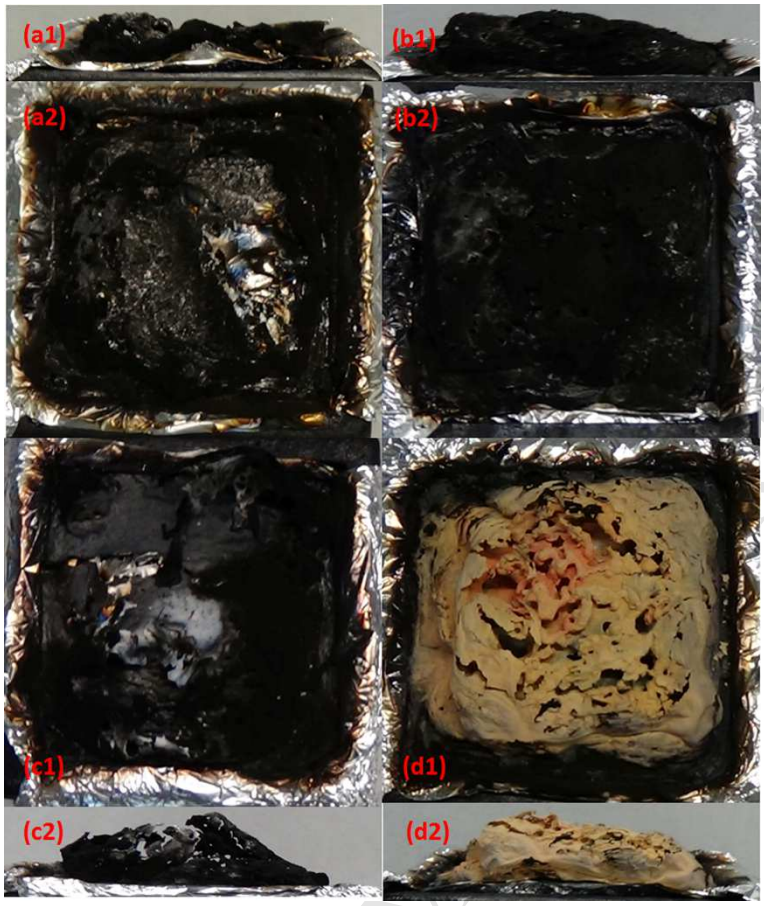

Fig.10. Digital images of (a1) side and (a2) top views of EP, (b1) side and (b2) top views of EP/6BN, (c1) top and (c2) side views of EP/6BN@PDA and (d1) top and (d2) side views of EP/6BN@PDA@Fe

3.5 Effluent study

The effluent evolution was analyzed via TG-FTIR with the intensity of evolved effluents exhibited in **Fig.11**. In **Fig.11** (a), the addition of BN and BN@PDA slightly reduced the peak intensity. In contrast, EP/6BN@DPA@Fe presented slightly increased peak intensity compared to those of EP/6BN and EP/6BN@PDA. However, at the late stage after 40s, EP/6BN@DPA@Fe possessed notably lower intensity than its counterparts, which was probably due to the higher charring capacity. Resultantly, in the integral curves of Gram-Schmidt curves (**Fig.11** (b)), EP/6BN@DPA@Fe exhibited remarkably reduced intensity value. The significant reduction of whole intensity at late stage and its integral value of BN@PDA@Fe showed that the hazard of evolved effluents was weakened. Moreover, the less effluent entered the flaming

zone, resulting in the lower fire intensity.

It was notable that in **Fig.11** (b), the integral curve of EP/6BN@PDA at 70min was lower than those of EP and EP/6BN, which was different from the order of THR in CCT. The underlying reason lied in the flammability of evolved products and the deteriorated char structure. In **Fig.6** (a), compared with EP and EP/6BN, the degradation stage to determine the less char yield of EP/6BN@PDA occurred at the late stage, which was attributed to the decomposition of newly-formed carbonaceous layers. Hence, at the higher temperature in TG (longer time in TG-FTIR), EP/6BN@PDA generated much more aromatic compounds relative to that of EP and nearly the identical amount compared with EP/6BN (**Fig S8**). Meanwhile, in the CCT, the barrier effect became stronger relative to the small-scale TG-FTIR analysis. The deterioration of barrier effect due to the continuous thermal degradation of PDA was supposed to be more pronounced, which resulted in the much release of flammable gases into the vapor phase. Therefore, it was reasonable that the flammability of evolved products of EP/6BN@PDA and the deteriorated barrier effect resulted in the increased total heat release.

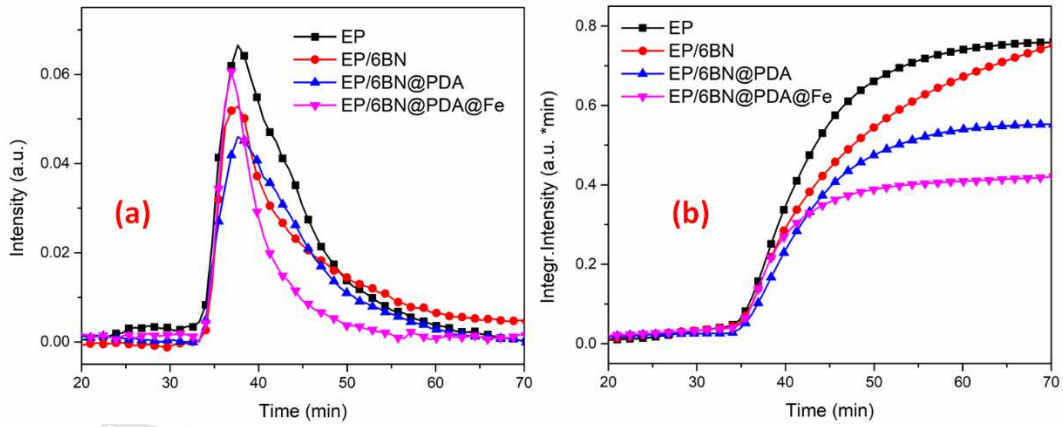

Fig.11 (a) Gram-Schmidt intensity curves and (b) integration curves of Gram-Schmidt curves of EP, EP/6BN, EP/6BN@PDA and EP/6BN@PDA@Fe

3.6 Fire-retardant mechanism

The fire-retardant mechanism (**Scheme 2**) in combination with increased thermal conductivity was proposed to account for improved fire safety and delayed TTI of

EP/6BN@PDA@Fe. After imposing heat on top surface, the heat was conducted to the underlying polymer. In consideration of higher thermal conductivity, the surface temperature increased more slowly than neat EP, which resulted in the higher TTI to reach the ignition temperature [38]. During combustion, the Fe nanocatalyst located at the interface of EP and BN strengthened the charring reaction toward integrity and a larger amount of char through the catalysis. The probable molecule-level interpretation was that iron atoms promoted the generation of polyaromatic compounds from the aliphatic and aromatic compounds based on the C-C coupling reaction [39, 40]. The generated char with undestroyed BN nanosheets as the reinforcement possessed stronger barrier effect towards oxygen, heat and flammable effluents [41]. Resultantly, heat release, smoke and CO production were improved in CCT. Conclusively, the fire retardancy associated with heat, smoke, CO and delayed ignition was enhanced after the sequential modification of BN with PDA and Fe nanocatalyst.

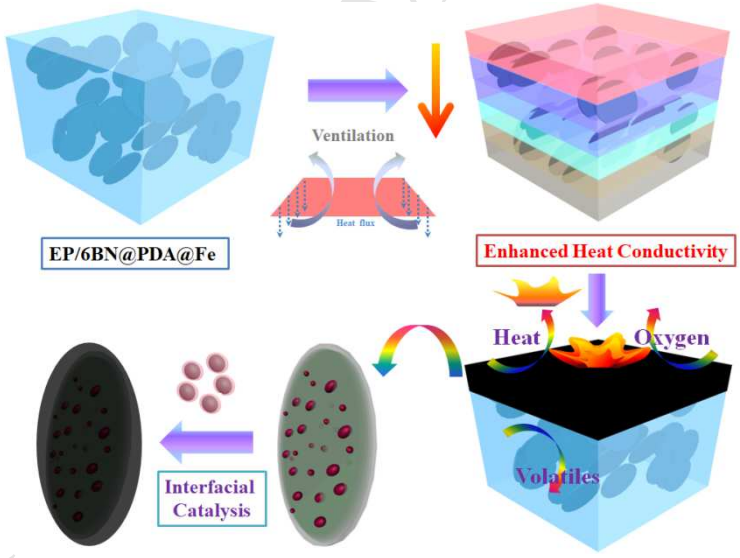

Scheme 2 The proposed fire-retardant mechanism for EP/6BN@PDA@Fe

4. Conclusion

In the manuscript, in order to improve fire retardancy of EP matrix, thermally exfoliated boron nitride nanosheets (BN) underwent the bio-inspired nanocoating of polydopamine (PDA) and interfacial growth of iron-derived nanocatalyst (Fe) to

prepare BN@PDA@Fe. Resultantly, the thermal conductivity of EP/6BN@PDA@Fe showed a notable enhancement of 39.9% compared with EP due to the improvement of dispersion. 6wt% BN@PDA@Fe imparted EP with enhanced LOI value by 10.0% and suppressed fire spread. Moreover, peak heat release rate of EP was reduced by 38.9% with remarkable reduction of CO and smoke production with BN@PDA@Fe. The optimization of char structure based on the interfacial catalytic charring accounted for the improved fire retardancy. The increased thermal conductivity to carry out excessive heat on the surface was proposed for delayed ignition. In perspective, the bioinspired interfacial engineering of BN offered a viable approach to improving fire safety of polymers.

Acknowledgements

This research is funded by Spanish Ministry of Economy and Competitiveness (MINECO) under Ramón y Cajal fellowship (RYC-2012-10737), COMETAD project (MAT2014-60435-C2-2-R) and COST Action CM1302 (Smart Inorganic Polymers). Likewise, the author was grateful to Dr. Juan Li, Dr. Miguel Castillo, Dr. Juan Pedro Fernández and Dr. José Sánchez del Río Saez in IMDEA Materials Institute for helpful discussion.

Notes and references

[1] Jin F-L, Li X, Park S-J. Synthesis and application of epoxy resins: A review. J Ind Eng Chem. 2015;29:1-11.

[2] Gérard C, Fontaine G, Bourbigot S. Synergistic and antagonistic effects in flame retardancy of an intumescent epoxy resin. Polym Advan Technol. 2011;22:1085-90.

[3] Tan Y, Shao Z-B, Yu L-X, Long J-W, Qi M, Chen L, et al. Piperazine-modified ammonium polyphosphate as monocomponent flame-retardant hardener for epoxy resin: flame retardance, curing behavior and mechanical property. Polym Chem. 2016;7:3003-12.

[4] Tang S, Qian L, Liu X, Dong Y. Gas-phase flame-retardant effects of a bi-group

compound based on phosphaphenanthrene and triazine-trione groups in epoxy resin. Polym Degrad Stabil. 2016;133:350-7.

[5] Wang P, Cai Z. Highly efficient flame-retardant epoxy resin with a novel DOPO-based triazole compound: Thermal stability, flame retardancy and mechanism. Polym Degrad Stabil. 2017;137:138-50.

[6] Wang X, Zhou S, Xing W, Yu B, Feng X, Song L, et al. Self-assembly of Ni–Fe layered double hydroxide/graphene hybrids for reducing fire hazard in epoxy composites. J Mater Chem A. 2013;1:4383-90.

[7] Li Z, Wang D-Y. Nano-architectured mesoporous silica decorated with ultrafine Co_3O_4 toward an efficient way to delaying ignition and improving fire retardancy of polystyrene. Mater Design. 2017; 129, 69-81.

[8] Carosio F, Laufer G, Alongi J, Camino G, Grunlan JC. Layer-by-layer assembly of silica-based flame retardant thin film on PET fabric. Polym Degrad Stabil. 2011;96:745-50.

[9] Beyer G. Short communication: carbon nanotubes as flame retardants for polymers. Fire Mater. 2002;26:291-3.

[10] Martins MS, Schartel B, Magalhães FD, Pereira C. The effect of traditional flame retardants, nanoclays and carbon nanotubes in the fire performance of epoxy resin composites. Fire Mater. 2017;41:111-30.

[11] Li Z, Liu Z, Dufosse F, Yan L, Wang D-Y. Interfacial engineering of layered double hydroxide toward epoxy resin with improved fire safety and mechanical property. Composites Part B: Engineering. 2018;152:336-346.

[12] Li Z, González AJ, Heeralal VB, Wang D-Y. Covalent assembly of MCM-41 nanospheres on graphene oxide for improving fire retardancy and mechanical property of epoxy resin. Composites Part B: Engineering. 2018;138:101-12.

[13] Dittrich B, Wartig KA, Hofmann D, Mülhaupt R, Schartel B. Carbon black, multiwall carbon nanotubes, expanded graphite and functionalized graphene flame retarded polypropylene nanocomposites. Polym Advan Technol. 2013;24:916-26.

[14] Yu B, Xing W, Guo W, Qiu S, Wang X, Lo S, et al. Thermal exfoliation of

hexagonal boron nitride for effective enhancements on thermal stability, flame retardancy and smoke suppression of epoxy resin nanocomposites via sol–gel process. J Mater Chem A. 2016;4:7330-40.

[15] Cai W, Hong N, Feng X, Zeng W, Shi Y, Zhang Y, et al. A facile strategy to simultaneously exfoliate and functionalize boron nitride nanosheets via Lewis acid-base interaction. Chem Eng J. 2017;330:309-21.

[16] Qu T, Yang N, Hou J, Li G, Yao Y, Zhang Q, et al. Flame retarding epoxy composites with poly (phosphazene-co-bisphenol A)-coated boron nitride to improve thermal conductivity and thermal stability. RSC Advances. 2017;7:6140-51.

[17] Wang D, Mu X, Cai W, Song L, Ma C, Hu Y. Constructing phosphorus, nitrogen, silicon-co-contained boron nitride nanosheets to reinforce flame retardant properties of unsaturated polyester resin. Composites Part A: Applied Science and Manufacturing. 2018;109:546-54.

[18] Rahatekar SS, Zammarano M, Matko S, Koziol KK, Windle AH, Nyden M, et al. Effect of carbon nanotubes and montmorillonite on the flammability of epoxy nanocomposites. Polym Degrad Stabil. 2010;95:870-9.

[19] Laoutid F, Bonnaud L, Alexandre M, Lopez-Cuesta J-M, Dubois P. New prospects in flame retardant polymer materials: from fundamentals to nanocomposites. Materials Science and Engineering: R: Reports. 2009;63:100-25.

[20] Kong Q, Wu T, Zhang J, Wang D-Y. Simultaneously improving flame retardancy and dynamic mechanical properties of epoxy resin nanocomposites through layered copper phenylphosphate. Compos Sci Technol. 2018;154:136-44.

[21] Jin W, Yuan L, Liang G, Gu A. Multifunctional cyclotriphosphazene/hexagonal boron nitride hybrids and their flame retarding bismaleimide resins with high thermal conductivity and thermal stability. ACS applied materials & interfaces. 2014;6:14931-44.

[22] Li Z, Liu L, González AJ, Wang D-Y. Bioinspired Polydopamine Induced Assembly of Ultrafine $Fe(OH)_3$ Nanoparticles on Halloysite toward Highly

Efficient Fire Retardancy of Epoxy Resin via An Action of Interfacial Catalysis. Polym Chem. 2017; 8, 3926-3936.

[23] Shen H, Guo J, Wang H, Zhao N, Xu J. Bioinspired modification of h-BN for high thermal conductive composite films with aligned structure. ACS applied materials & interfaces. 2015;7:5701-8.

[24] Cui Z, Oyer AJ, Glover AJ, Schniepp HC, Adamson DH. Large scale thermal exfoliation and functionalization of boron nitride. Small. 2014;10:2352-5.

[25] Thakur VK, Yan J, Lin M-F, Zhi C, Golberg D, Bando Y, et al. Novel polymer nanocomposites from bioinspired green aqueous functionalization of BNNTs. Polym Chem. 2012;3:962-9.

[26] Zheng X, Zhang J, Wang J, Qi X, Rosenholm JM, Cai K. Polydopamine coatings in confined nanopore space: toward improved retention and release of hydrophilic cargo. The Journal of Physical Chemistry C. 2015;119:24512-21.

[27] Guo J, Wang R, Tjiu WW, Pan J, Liu T. Synthesis of Fe nanoparticles@ graphene composites for environmental applications. J Hazard Mater. 2012;225:63-73.

[28] Chen H, Cao Y, Wei E, Gong T, Xian Q. Facile synthesis of graphene nano zero-valent iron composites and their efficient removal of trichloronitromethane from drinking water. Chemosphere. 2016;146:32-9.

[29] Li Z, Expósito DF, González AJ, Wang D-Y. Natural halloysite nanotube based functionalized nanohybrid assembled via phosphorus-containing slow release method: A highly efficient way to impart flame retardancy to polylactide. Eur Polym J. 2017;93:458-70.

[30] Fu J, Chen Z, Wang M, Liu S, Zhang J, Zhang J, et al. Adsorption of methylene blue by a high-efficiency adsorbent (polydopamine microspheres): kinetics, isotherm, thermodynamics and mechanism analysis. Chem Eng J. 2015;259:53-61.

[31] Yang L, Phua SL, Teo JKH, Toh CL, Lau SK, Ma J, et al. A biomimetic approach to enhancing interfacial interactions: polydopamine-coated clay as reinforcement for epoxy resin. ACS applied materials & interfaces. 2011;3:3026-32.

[32] Wang D-Y, Das A, Leuteritz A, Boldt R, Häußler L, Wagenknecht U, et al.

Thermal degradation behaviors of a novel nanocomposite based on polypropylene and Co–Al layered double hydroxide. Polym Degrad Stabil. 2011;96:285-90.

[33] Alongi J, Han Z, Bourbigot S. Intumescence: tradition versus novelty. A comprehensive review. Prog Polym Sci. 2015;51:28-73.

[34] Zhao X, Gao S, Liu G. A THEIC-based polyphosphate melamine intumescent flame retardant and its flame retardancy properties for polylactide. J Anal Appl Pyrol. 2016;122:24-34.

[35] Pappalardo S, Russo P, Acierno D, Rabe S, Schartel B. The synergistic effect of organically modified sepiolite in intumescent flame retardant polypropylene. Eur Polym J. 2016;76:196-207.

[36] Schartel B, Hull TR. Development of fire□retarded materials—Interpretation of cone calorimeter data. Fire Mater. 2007;31:327-54.

[37] Li Z, Zhang J, Dufosse F, Wang D-Y. Ultrafine nickel nanocatalyst-engineering of an organic layered double hydroxide towards a super-efficient fire-safe epoxy resin via interfacial catalysis. J Mater Chem A. 2018;6:8488-98.

[38] Fina A, Cuttica F, Camino G. Ignition of polypropylene/montmorillonite nanocomposites. Polym Degrad Stabil. 2012;97:2619-26.

[39] Zhang J, Kong Q, Wang D-Y. Simultaneously improving the fire safety and mechanical properties of epoxy resin with Fe-CNTs via large-scale preparation. J Mater Chem A. 2018;6:6376-86.

[40] Sapountzis I, Lin W, Kofink CC, Despotopoulou C, Knochel P. Iron□Catalyzed Aryl-Aryl Cross□Couplings with Magnesium□Derived Copper Reagents. Angewandte Chemie International Edition. 2005;44:1654-8.

[41] Wang X, Kalali E N, Wang D-Y. Renewable cardanol-based surfactant modified layered double hydroxide as a flame retardant for epoxy resin. ACS Sustainable Chemistry & Engineering, 2015, 3: 3281-3290.

Highlights

1. Exfoliated BN was hierarchically modified with polydopamine and iron derivatives

2. The targeted BN@PDA@Fe showed better dispersion than its counterparts in epoxy resin.

3. BN@PDA@Fe efficiently suppressed integral fire hazard of epoxy resin.

4. Ignition of epoxy resin was delayed based on the increased thermal conductivity.

5. Interfacially catalytic charring toward high-quality char accounted for fire safety.